

Article

Reversible Single-Crystal-to-Single-Crystal Structural Transformation in a Mixed-Ligand 2D Layered Metal-Organic Framework: Structural Characterization and Sorption Study

Chih-Chieh Wang ^{1,*}, Szu-Yu Ke ¹, Kuan-Ting Chen ¹, Yi-Fang Hsieh ¹, Tzu-Heng Wang ¹, Gene-Hsiang Lee ² and Yu-Chun Chuang ^{3,*} 

¹ Department of Chemistry, Soochow University, Taipei 11102, Taiwan; sarah6017@yahoo.com.tw (S.-Y.K.); 04133019@scu.edu.tw (K.-T.C.); fangfangmimai@gmail.com (Y.-F.H.); 06333002@scu.edu.tw (T.-H.W.)

² Instrumentation Center, National Taiwan University, Taipei 10617, Taiwan; ghlee@ntu.edu.tw

³ National Synchrotron Radiation Research Center, Hsinchu 30076, Taiwan

* Correspondence: ccwang@scu.edu.tw (C.-C.W.); chuang.yc@nsrrc.org.tw (Y.-C.C.); Tel.: +886-2-2881-9471 (ext. 6828) (C.-C.W.)

Academic Editor: George E. Kostakis

Received: 20 November 2017; Accepted: 5 December 2017; Published: 7 December 2017

Abstract: A 3D supramolecular network, [Cd(bipy)(C₄O₄)(H₂O)₂] \cdot 3H₂O (**1**) (bipy = 4,4'-bipyridine and C₄O₄²⁻ = dianion of H₂C₄O₄), constructed by mixed-ligand two-dimensional (2D) metal-organic frameworks (MOFs) has been reported and structurally determined by the single-crystal X-ray diffraction method and characterized by other physicochemical methods. In **1**, the C₄O₄²⁻ and bipy both act as bridging ligands connecting the Cd(II) ions to form a 2D layered MOF, which are then extended to a 3D supramolecular network via the mutually parallel and interpenetrating arrangements among the 2D-layered MOFs. Compound **1** shows a two-step dehydration process with weight losses of 11.0% and 7.3%, corresponding to the weight-loss of three guest and two coordinated water molecules, respectively, and exhibits an interesting reversible single-crystal-to-single-crystal (SCSC) structural transformation upon de-hydration and re-hydration for guest water molecules. The SCSC structural transformation have been demonstrated and monitored by single-crystal and X-ray powder diffraction, and thermogravimetric analysis studies.

Keywords: coordination polymer; metal-organic framework; SCSC structural transformation; hydrogen bond; gas sorption

1. Introduction

Porous materials based on coordination polymers (CPs), or metal-organic frameworks (MOFs) [1,2] containing guest molecules are very attractive research field, not only owing to their designable structure, unusual flexibilities, but also on their tunable functional application [3–12]. In this field, dynamic porosity has been paid much attention on the structural characteristics, as well as on the function of guest inclusions [13–25]. In order to increase the flexibility of the porosity for guest inclusion, the design of host framework with a flexible skeleton is required. Based on this requirement, the dimensionality of host framework and binding forces for the component skeleton becomes an important target. A variety of supramolecular architectures have been built up with a large range of bonding forces, depending on the system, the interactions can range from M–L coordination bonds, to strong halogen [26–32] or hydrogen bonds [31,32], to much weaker forces, such as weak hydrogen bonds [33,34] and π – π stacking of small aromatics [35–39]. N,N-based ligands, such as 4,4'-bipyridine (bipy) and pyrazine, have been widely used on the construction of

many MOFs, including diamondoid, honeycomb, grid, T-shape, ladder, brick-wall, and octahedral frameworks [40–48]. In the previous study, a series of interpenetrated metal-organic coordination complexes, $\{[M(C_4O_4)(bipy)(H_2O)_2] \cdot 3H_2O\}_\infty$ ($M = Mn, Fe, Co, Ni$; $C_4O_4^{2-}$ = dianion of $H_2C_4O_4$), have been synthesized under hydrothermal condition. The reversible de-/rehydration processes of guest water molecules in the 1D channels by heating or by vacuum were accompanied with color-changing and structural variation of the materials, which have been identified by MS measurements, UV spectrometry, and X-ray powder diffraction methods [49–51]. In our previous study [52], an isostructural coordination polymer, $\{[Cd(C_4O_4)(bipy)(H_2O)_2] \cdot 3H_2O\}_n$ (**1**), has been synthesized under hydrothermal conditions and its reversible de-/rehydration property of guest water molecules in channels accompanying structural variation is demonstrated by thermogravimetric (TG) analysis, as well as temperature-dependent power X-ray diffraction. However, the detail structural information on the single-crystal-to-single-crystal (SCSC) transformation associated with the de-/rehydration of the guest water molecules in the channels, the second stage water de-/adsorption behavior of the coordinated water molecules, and the gas sorption property of **1** are interesting and worthy of further study. With our continuous effort on the structural transformation study of the two-step water de-/adsorption behavior in **1**, we report here on the exploration of the relationship between the structures and de-/rehydration behavior. The dehydrated species $\{[Cd(C_4O_4)(bipy)(H_2O)_2]\}_n$ (**1a**), after heating **1** at 90 °C, show CO_2 gas sorption uptakes. Compound **1a** also shows remarkable reversibility to give rehydrated $\{[Cd(C_4O_4)(bipy)(H_2O)_2] \cdot 3H_2O\}_n$ (**1b**), which is the same to parent **1**, when exposed to water vapor.

2. Results and Discussion

In the study, compound **1** was synthesized by solution method instead of hydrothermal method reported in previous study [52]. The reaction yield is obviously improved from 23.4% under hydrothermal condition to 70.4% by the solution method. The most relevant IR features are those associated with the chelating squarate ligands. Strong and broad absorptions occurring in the range of 1603–1323 cm^{-1} centered at 1470 cm^{-1} for **1** are characteristic of $C_4O_4^{2-}$ ions [53], which can be assigned to the vibrational modes representing mixtures of C–O and C–C stretching motions.

2.1. Structural Description of **1**

The crystal structure of **1**, synthesized by the solution method, is re-determined and is almost the same as the crystal structure described in our previous report [52], with a 3D microporous supramolecular network being constructed by 2D-layered MOFs. The related bond lengths and angles around the Cd(II) ion are listed in Table 1. The squarate and bipy both act as a bridging ligand with $\mu_{1,3}$ -*bis*-monodentate and *bis*-monodentate coordination mode, respectively, leading the formation of a 2D layered MOF (Figure 1b) along the *b* axis. The 2D MOF of **1** can be viewed in a simplified way using TOPOS [54,55] as a four-connected uninodal net with the point symmetry (Schläfli symbol) $\{4^4.6^2\}$. Adjacent 2D layers are arranged in mutually parallel and interpenetrated manners to complete its 3D supramolecular network, which generates 1D channels along the *c* axis intercalated with guest water molecules (Figure 1c). Hydrogen bonding interaction plays an important role on the stabilization of the 3D supramolecular network. In the crystal packing, the coordinated water molecules (O(3)) are held together with uncoordinated oxygen atoms (O(2)) of squarate ($C_4O_4^{2-}$) by means of intramolecular O–H \cdots O hydrogen bonds with O \cdots O distances of 2.664(5) and 2.698(5). The 3D supramolecular architecture is further reinforced by the O–H \cdots O hydrogen bonds among the guest water molecules (O(4) and O(5)) and squarate ligands. Related bond distances and angles of O–H \cdots O hydrogen bonds are listed in Table 2.

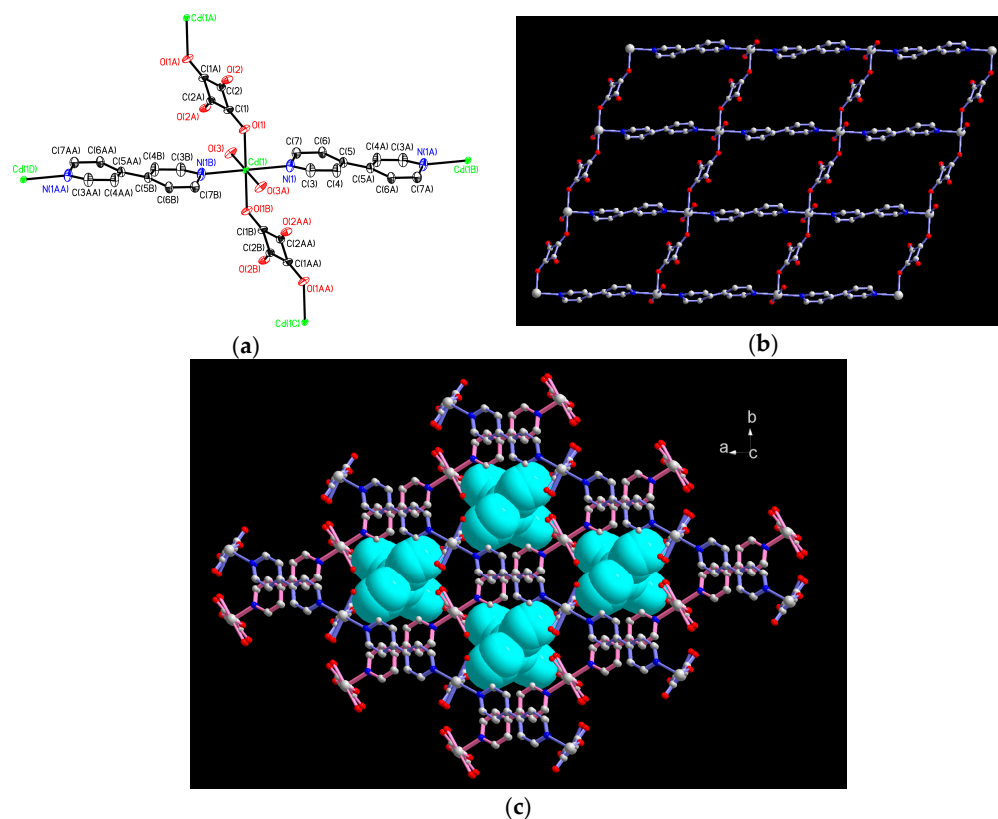


Figure 1. (a) Coordination environment of the Cd(II) ion in **1** with atom labelling scheme (ORTEP drawing, 50% thermal ellipsoids). The guest water molecules and H atoms are omitted for clarity. (b) The 2D MOF in **1** via the bridges of squarate and 4,4'-bipyridine; (c) The 3D supramolecular network with the 1D channels intercalated with guest water molecules (space-filling mode) viewing along the *c* axis.

Table 1. Bond lengths (Å) and angles (°) around Zn(II) ion in **1**, **1a**, and **1b**.¹

Compound	1	1a	1b
Cd(1)–O(3)	2.264(3)	2.303(3)	2.265(2)
Cd(1)–O(3) _{<i>i</i>}	2.264(3)	2.303(3)	2.265(2)
Cd(1)–O(1)	2.294(3)	2.273(2)	2.296(2)
Cd(1)–O(1) _{<i>i</i>}	2.294(3)	2.273(2)	2.296(2)
Cd(1)–N(1)	2.341(4)	2.339(3)	2.340(2)
Cd(1)–N(1) _{<i>i</i>}	2.341(4)	2.339(3)	2.340(2)
O(3)–Cd(1)–O(3) _{<i>i</i>}	180	180.0	180.0
O(3) _{<i>i</i>} –Cd(1)–O(1) _{<i>i</i>}	92.77(12)	93.61(11)	92.76(7)
O(3)–Cd(1)–O(1) _{<i>i</i>}	87.23(12)	86.39(11)	87.24(7)
O(3) _{<i>i</i>} –Cd(1)–O(1)	87.23(12)	86.39(11)	87.24(7)
O(3)–Cd(1)–O(1)	92.77(12)	93.61(11)	92.76(7)
O(1)–Cd(1)–O(1) _{<i>i</i>}	180	180.0	180.0
O(3) _{<i>i</i>} –Cd(1)–N(1)	87.82(13)	91.88(11)	87.93(8)
O(3)–Cd(1)–N(1)	92.18(13)	88.12(11)	92.07(8)
O(1) _{<i>i</i>} –Cd(1)–N(1)	85.78(14)	86.46(11)	85.60(8)
O(1)–Cd(1)–N(1)	94.22(14)	93.54(11)	94.40(8)
O(3) _{<i>i</i>} –Cd(1)–N(1) _{<i>i</i>}	92.18(13)	88.12(11)	92.07(8)
O(3)–Cd(1)–N(1) _{<i>i</i>}	87.82(13)	91.88(11)	87.93(8)
O(1) _{<i>i</i>} –Cd(1)–N(1) _{<i>i</i>}	94.22(14)	93.54(11)	94.40(8)
O(1)–Cd(1)–N(1) _{<i>i</i>}	85.78(14)	86.46(11)	85.60(8)
N(1)–Cd(1)–N(1) _{<i>i</i>}	180.0	180.0	180.0

¹ Symmetry transformations used to generate equivalent atoms: *i* = $-x + 1/2, -y + 1/2, -z + 1$.

Table 2. The O–H···O hydrogen bonds for **1** and **1b**, respectively. ¹

Compound 1				
D–H···A	D–H (Å)	H···A (Å)	D···A (Å)	∠ D–H···A (°)
O(3)–H(3A)···O(2) _i	0.81(7)	1.88(7)	2.664(5)	162(6)
O(3)–H(3B)···O(2) _{ii}	0.87(7)	1.85(7)	2.698(5)	163(6)
O(4)–H(4A)···O(5)	0.83(5)	1.96(5)	2.762(5)	162(6)
O(5)–H(5A)···O(1)	0.71(8)	2.11(8)	2.807(5)	171(8)
O(5)–H(5B)···O(4) _{iii}	0.79(7)	2.00(7)	2.782(5)	168(7)
Compound 1b				
D–H···A	D–H (Å)	H···A (Å)	D···A (Å)	∠ D–H···A (°)
O(3)–H(3A)···O(2) _i	0.79(4)	1.89(4)	2.663(3)	166(4)
O(3)–H(3B)···O(2) _{ii}	0.81(4)	1.91(4)	2.698(3)	165(3)
O(4)–H(4A)···O(5)	0.82(3)	1.95(3)	2.766(3)	169(4)
O(5)–H(5A)···O(1)	0.81(4)	2.01(4)	2.808(3)	171(4)
O(5)–H(5B)···O(4) _{iii}	0.76(4)	2.04(4)	2.783(3)	168(4)

¹ Symmetry transformations used to generate equivalent atoms: $i = -x + 1/2, -y + 1/2, -z$; $ii = -x + 1/2, y - 1/2, -z + 1/2$; $iii = -x + 1, -y + 1, -z + 1$.

2.2. Water Adsorption Property of (**1**) by Cyclic TG Analysis and PXRD Measurements

In our previously thermal-stability study [52], the weight losses of the first and second steps were 11.1% and 7.7%, corresponding to the release of three guest water molecules (calc. 11.5%) and two coordinated water molecules (calc. 7.7%), respectively, and the first weight-loss step has been proven to be a reversible de-/adsorption of three guest water molecules by cyclic TG measurements under water vapor, as demonstrated by the display of de-/rehydration processes as a function of time and temperature [52]. This result can be correlated to the polarity of the pore surfaces, as the framework is adorned with high affinity for H₂O due to the presence of hydrophilic sites of C₄O₄²⁻ ligands. Unlike the complete reversibility of guest water molecules in the first stage, the removal of coordinated water molecules is more likely to be only partially reversible in the second stage (Figure 2). When the guest and coordinated water molecules are completely removed with the weight loss of 18.8% after the temperature reaching 170 °C, only partial weight increase of 2.7% under water vapor has been recovered during the cooling process. Such heating and cooling processes have been repeated for five cycles (Figure 2) with weight-increasing and weight-decreasing percentages in the range of 2.7–3.2% to demonstrate the stable but incomplete water ad-/desorption behavior during the thermal re-/dehydration processes. This result indicates that, during the de-hydration period, the 3D supramolecular network and the coordination environment of Cd(II) ions of completely dehydrated form **1** might be changed after the removal of coordinated water molecules and may not be easily recovered to the original structure, which will be discussed in the next powder X-ray diffraction part.

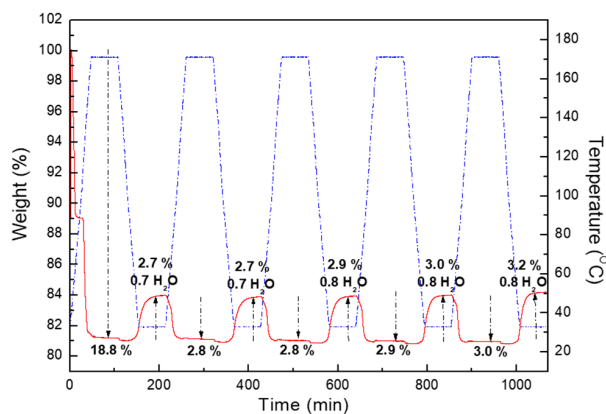


Figure 2. The cyclic TG measurements of water de-/adsorption processes at 170 °C and back to RT. Red solid line: the variation of weight loss with time; blue dashed line: the variation of temperature with time.

According to the TGA and single crystal diffraction results, the first structure change are dominated from packing guest water molecules loss and the second step is triggered by coordinated water molecules loss. To confirm the water re-absorption behavior, an in situ powder X-ray diffraction experiment was performed and shown in Figure 3. The sample in glass capillary was heated up to 90 °C initially and stays 5 min to remove the packing water molecules. Compare to the simulation pattern of rehydrated **1a** at 340 K, the diffraction pattern show the first step packing guest water molecules loss has been happened. Then the sample was taken into water and re-measured powder pattern at 30 °C. Clearly, the structure can be recovered effectively. However, it was failed to recover the structure while the coordinated water molecules be removed. A very large structure change occurred at the second water molecules loss step, which leads to an irreversible reaction.

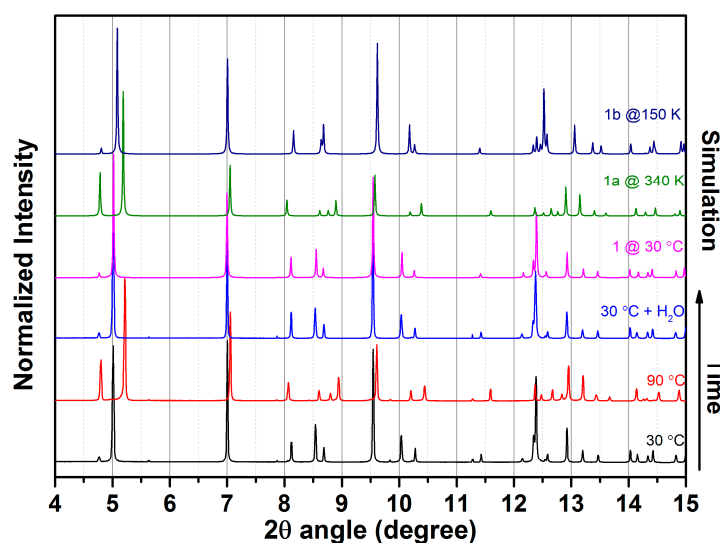
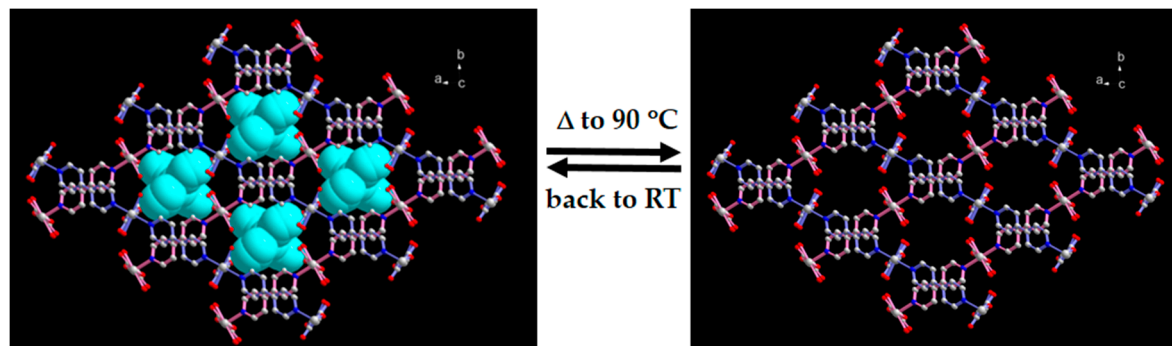


Figure 3. PXRD patterns of as synthesized **1** at RT (black), dehydrated **1a** at 90 °C (red), rehydrated **1b** at RT (blue), simulated **1** from single-crystal data (pink), simulated **1a** from single-crystal data at 90 °C (green), and simulated **1b** from single-crystal data at RT (deep blue).

2.3. SCSC Transformation Associated with Guest Water De-/Rehydration

According to the TG analysis and in situ PXRD measurements, the guest water molecules located into the channels can be removed from the host framework by heating up to 90 °C. The 3D supramolecular architecture of dehydrated **1** is rigid and stable without the guest water molecules, and the de-/adsorption processes of guest water molecules are reversible. Moreover, the thermal stability of the framework provides the opportunity to determine the crystal structure of dehydrated **1a** after the removal of guest water molecules from the host framework by controlled the heating condition and crystal structure of the re-hydration **1b** with the dehydrated **1a** upon exposure to water vapor at RT. Single-crystal-to-single-crystal transformation experiments were performed by single-crystal X-ray diffraction method, which give the structures of dehydrated $[\text{Cd}(\text{C}_4\text{O}_4)(\text{bipy})(\text{H}_2\text{O})_2]_n$ (**1a**) and rehydrated $\{[\text{Cd}(\text{C}_4\text{O}_4)(\text{bipy})(\text{H}_2\text{O})_2] \cdot 3\text{H}_2\text{O}\}_n$ (**1b**), respectively, with very similar cell parameters (Table 3). The structure of the dehydrated **1a** reveals that the 3D supramolecular architecture framework is nearly the same as that of **1** with the difference only on the nonexistence of guest water molecules. The related bond lengths and angles around the Cd(II) ion are similar to that of **1** with little difference (Table 1). Furthermore, when the dehydrated **1a** were exposed to water vapor at RT, structural determination reveals that **1a** re-absorbed water molecules to generate a rehydrated $\{[\text{Cd}(\text{C}_4\text{O}_4)(\text{bipy})(\text{H}_2\text{O})_2] \cdot 3\text{H}_2\text{O}\}_n$ (**1b**), showing a complete reversibility of de-/rehydration processes in the 3D supramolecular network as shown in Scheme 1. The related bond lengths and angles around Cd(II) ion are also in comparable with those of **1** (Table 1). It is important to note that hydrogen bonds existing between the guest water molecules and the host framework found in the rehydrated **1b** are

almost the same as those found in **1** (Table 2). This result indicates that hydrogen bonding interaction play a key role on the SCSC transformation mechanism of reversible de-/rehydration and provide a memorial tracing pathway for the guest water during the guest water absorption process.



Scheme 1. SCSC structural transformation between **1** and **1a** during the reversible de-/rehydration processes.

Table 3. Crystal data and refinement details of compounds **1**, **1a** and **1b**.

Compound	1	1a	1b
empirical formula	C ₁₄ H ₁₈ Cd ₁ N ₂ O ₉	C ₁₄ H ₁₂ Cd ₁ N ₂ O ₆	C ₁₄ H ₁₈ Cd ₁ N ₂ O ₉
formula mass (g mol ⁻¹)	470.70	416.66	470.70
crystal system	Monoclinic	Monoclinic	Monoclinic
space group	C 2/c	C 2/c	C 2/c
<i>a</i> (Å)	20.3421(8)	19.7226(10)	20.3589(12)
<i>b</i> (Å)	11.6164(5)	11.7865(5)	11.6195(6)
<i>c</i> (Å)	8.3198(3)	8.1877(3)	8.3196(4)
α (deg)	90	90	90
β (deg)	113.7456(15)	112.1639(15)	113.7461(18)
γ (deg)	90	90	90
<i>V</i> (Å ³)	1799.55(12)	1762.68(13)	1801.47(17)
<i>Z</i>	4	4	4
<i>T</i> (K)	150(2)	340(2)	150(2)
<i>D</i> _{calcd} (g cm ⁻³)	1.737	1.570	1.736
μ (mm ⁻¹)	1.263	1.267	1.262
θ range (deg)	2.066–27.474	2.230–27.484	3.011–27.491
total no. of data collected	5780	5760	6113
no. of unique data	2070	2028	2066
no. of obsd data (<i>I</i> > 2 σ (<i>I</i>))	1681	1594	1649
<i>R</i> _{int}	0.0334	0.0318	0.0274
refine params	145	114	145
<i>R</i> ₁ , <i>wR</i> ₂ (<i>I</i> > 2 σ (<i>I</i>)) ¹	0.0360, 0.0924	0.0389, 0.0733	0.0250, 0.0482
<i>R</i> ₁ , <i>wR</i> ₂ (all data) ¹	0.0464, 0.1003	0.0551, 0.0800	0.0376, 0.0537
GOF ²	1.085	1.191	1.095

¹ $R_1 = \sum ||F_o - F_c| | / \sum |F_o|$; $wR_2(F^2) = [\sum w |F_o^2 - F_c^2|^2 / \sum w (F_o^4)]^{1/2}$. ² GOF = $[\sum [w |F_o^2 - F_c^2|^2] / (n - p)]^{1/2}$.

2.4. Adsorption Properties of (**1**)

Encouraged by the structural flexibility of **1**, the gas uptake capacities of the dehydrated (activated) framework are determined. Before the measurements, powder samples of compound **1** were evacuated at 90 °C for 24 h to obtain the activated form **1a** (removal of three guest water molecules). The isotherm obtained with N₂ gas at 78 K revealed a typical Type-II adsorption profile with very low uptake, suggesting only surface adsorption. (Figure 4a). Surprisingly, even though **1** is nonporous towards to N₂, we found that it is porous towards CO₂ at 198 K. The CO₂ adsorption isotherms at 198 K for **1a** exhibit a typical Type-I adsorption behavior (Figure 4b) with the adsorption uptake of 18.3 cm³ g⁻¹.

The adsorption capability of **1** for CO₂ gases is low, but significant. In order to understand the interactions of guest water molecules with the host framework, the water vapor adsorption behavior of the activated **1a** under ambient condition is measured. The activated **1a** show high H₂O uptake (~43.5 cm³ g⁻¹) at lower P/P_0 (0.0–0.1), and the final uptake amount reaches 82.6 cm³ g⁻¹, which corresponds to 2.6 molecules of H₂O per formula unit (Figure 4c).

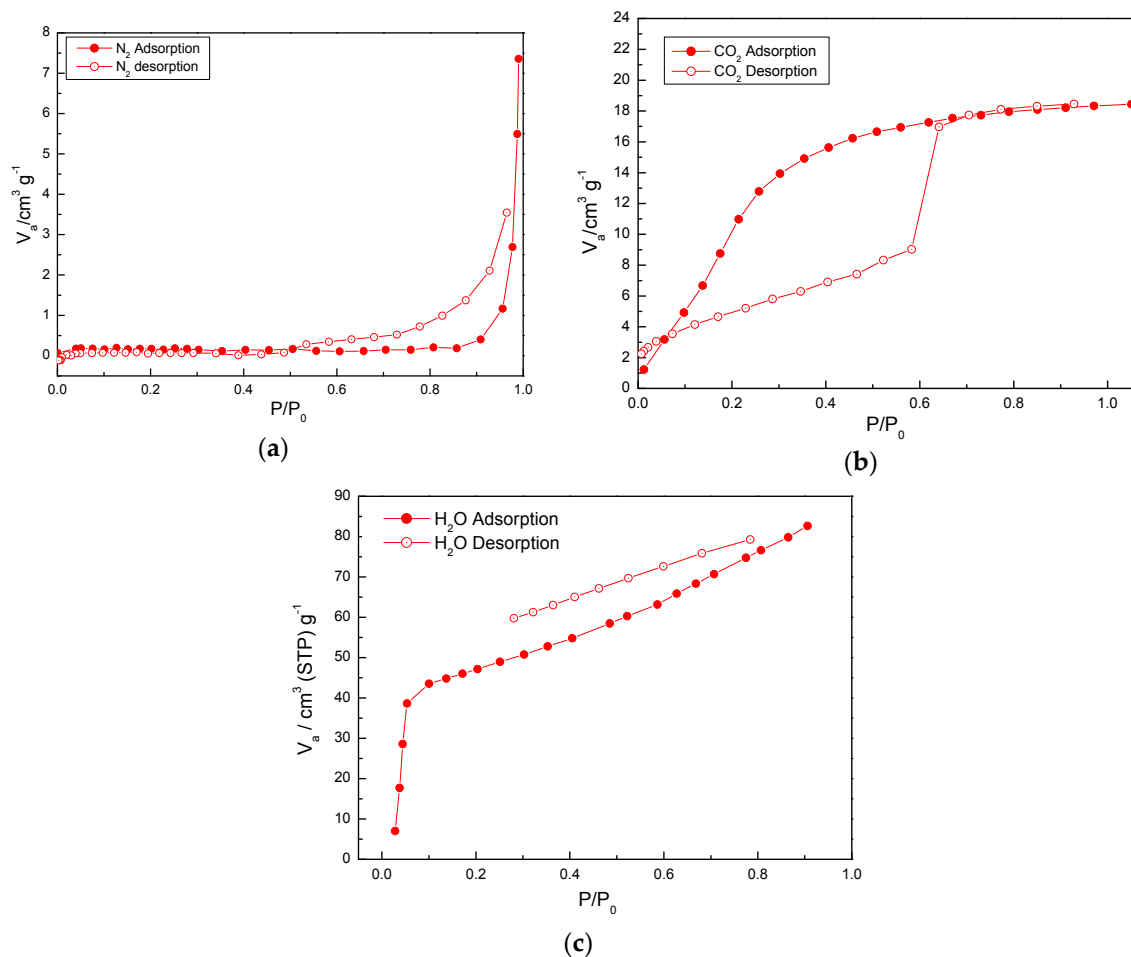


Figure 4. (a) N₂ adsorption and desorption isotherms measured at 77 K; (b) CO₂ adsorption and desorption isotherms measured at 198 K; and (c) H₂O adsorption and desorption isotherms measured at 298 K.

3. Materials and Methods

3.1. Materials and Physical Techniques

All chemicals were of reagent grade and were used as commercially obtained without further purification. Elementary analyses (carbon, hydrogen, and nitrogen) were performed using a Perkin-Elmer 2400 elemental analyzer. IR spectra were recorded on a Nicolet Fourier Transform IR, MAGNA-IR 500 spectrometer in the range of 500–4000 cm⁻¹ using the KBr disc technique. Thermogravimetric analysis (TGA) of compounds **1** was performed on a computer-controlled Perkin-Elmer 7 Series/UNIX TGA7 analyzer. Single-phased powder samples were loaded into alumina pans and heated with a ramp rate of 5 °C/min from room temperature to 800 °C under a nitrogen atmosphere. The adsorption isotherm of N₂ (77 K) and CO₂ (200 K) for **1** was measured in the gaseous state by using BELSORP-max volumetric adsorption equipment from BEL, Osaka, Japan. In the sample cell (~1.8 cm³) maintained at $T \pm 0.03$ K was placed the adsorbent sample (~100–150 mg), which has

been prepared at 90 and 180 °C for **1** and 10^{-2} Pa for about 24 h prior to measurement of the isotherm. The adsorbate was placed into the sample cell, and then the change of pressure was monitored and the degree of adsorption was determined by the decrease of pressure at equilibrium state. All operations were through automatically computer-controlled.

3.2. Synthesis of $\{[Cd(C_4O_4)(bipy)(H_2O)_2] \cdot 3H_2O\}_\infty$ (**1**), Dehydrated $\{[Cd(C_4O_4)(bipy)(H_2O)_2]\}_\infty$ (**1a**) and Rehydrated $\{[Cd(C_4O_4)(bipy)(H_2O)_2] \cdot 3H_2O\}_\infty$ (**1b**)

An ethanol/H₂O solution (1:1, 50 mL) of H₂C₄O₄ (0.1419 g, 0.0012 mol) was added to an ethanol/water (1:1, 100 mL) solution of Cd(NO₃)₂·4H₂O (0.4107 g, 0.0025 mol) and 4,4'-bipyridine (0.3904 g, 0.0013 mmol) at room temperature. After standing for one week, colorless needle-like crystals of **1** (yield, 0.412g 70.4%) were obtained which are suitable for X-ray diffraction analysis. Anal. Calc. for C₁₄H₁₂N₂O₆Cd₁ (**1**): C 35.21, N 5.74, H 3.95; Found: C 35.69, N 5.94, H 3.82. IR (KBr pellet): $\nu = 1603$ (m), 1471 (s), 1413 (s), 1323 (m), 1221 (m), 1067 (m), 1006 (m), 672 (s), 628 (vs) cm⁻¹. The fresh crystals of **1** are heated at 90 °C to obtain dehydrated crystals $\{[Cd(C_4O_4)(bipy)(H_2O)_2]\}_\infty$ (**1a**). The dehydrated crystals **1a** are then stand at RT for one day to obtain rehydrated crystals $\{[Cd(C_4O_4)(bipy)(H_2O)_2] \cdot 3H_2O\}_\infty$ (**1b**).

3.3. Crystallographic Data Collection and Refinements

Single-crystal structure analysis for compound **1**, **1a**, and **1b** were performed out on a Siemens SMART diffractometer (Taipei, Taiwan) with a CCD detector with Mo radiation ($\lambda = 0.71073$ Å) at 150 K for **1** and **1b** and at 340 K for **1a**, respectively. A preliminary orientation matrix and unit cell parameters were determined from three runs of 15 frames each, each frame correspond to a 0.3° scan in 10 s, following by spot integration and least-squares refinement. For each structure, data were measured using ω scans of 0.3° per frame for 20 s until a complete hemisphere had been collected. Cell parameters were retrieved using SMART [56] software (Bruker SAINT) and refined with SAINT (Bruker SAINT) [57] on all observed reflections. Data reduction was performed with the SAINT [58] software package and corrected for Lorentz and polarization effects. Absorption corrections were applied with the program SADABS (Bruker, 2016) [58]. Direct phase determination and subsequent difference Fourier map synthesis yielded the positions of all atoms, which were subjected to anisotropic refinements for non-hydrogen atoms and isotropic for hydrogen atoms. The final full-matrix, least-squares refinement on F^2 was applied for all observed reflections [$I > 2\sigma(I)$]. All calculations were performed by using the SHELXL-2014/7 software package [59]. Crystal data and details of the data collection and structure refinements for **1–4** are summarized in Table 1. CCDC-1584569, 1584570, and 1584571 for **1**, **1a**, and **1b** contains the supplementary crystallographic data for this paper. These data can be obtained free of charge at www.ccdc.cam.ac.uk/conts/retrieving.html (or from the Cambridge Crystallographic Data Centre, 12, Union Road, Cambridge CB2 1EZ, UK; fax: (internat.) +44-1223/336-033; email: deposit@ccdc.cam.ac.uk).

3.4. In Situ X-ray Powder Diffraction

Variable temperature synchrotron powder X-ray diffraction data were collected at the Taiwan Photon Source of the National Synchrotron Radiation Research Center (TPS 09A, Hsinchu, Taiwan). The 15 keV X-ray source is delivered from an in-vacuum undulator (IU22, Hsinchu, Taiwan) and the powder diffraction patterns were recorded by a position-sensitive detector, MYTHEN 24K (Hsinchu, Taiwan), covering a 2θ range of 120°. All powder samples were loaded into 0.3 mm capillary. To obtain better random orientation, the capillary was rotated at 400 RPM during data collection. For high temperature experiment, a hot air gas blower was placed 2 mm under the sample. Due to the small gaps between detector modules, the two data sets were collected 2° apart with 60 s exposure time and the data were merged and gridded to give a continuous dataset.

3.5. Measurements of Gas Adsorption of Activated **1a**

The adsorption isotherms of N₂ (77 K), CO₂ (198 K) and H₂O (298 K) were measured in the gaseous state by using BELSORP-max volumetric adsorption equipment from BEL, Osaka, Japan. In the sample cell (~1.8 cm³) maintained at T ± 0.03 K was placed the adsorbent sample (~100–150 mg), which has been prepared at 90 °C for **1a** and 10^{−2} Pa for about 24 h prior to measurement of the isotherm. The adsorbate was placed into the sample cell, and then the change of pressure was monitored and the degree of adsorption was determined by the decrease of pressure at equilibrium state. All operations were through automatically computer-controlled.

4. Conclusions

A 3D supramolecular network, {[Cd(C₄O₄)(bipy)(H₂O)₂]}·3H₂O)_n (**1**), constructed by 2D-layered MOFs has been successfully synthesized. Adjacent 2D layers were then self-assembled via the mutually parallel and interpenetrating manners to form a 3D supramolecular network. Hydrogen bonding interaction among uncoordinated oxygen of squarate, coordinated water molecules in the host framework and the guest water molecules provide extra-energy on the stabilization of the 3D supramolecular architecture of **1**. The guest water molecules in the as-synthesized samples can be removed readily by heating the sample to obtain dehydrated [Cd(C₄O₄)(bipy)(H₂O)₂]_n (**1a**), and this resulting microporous material is highly robust and chemically inert. Noteworthy, compound **1** shows an interesting SCSC structural transformation between the dehydrated [Cd(C₄O₄)(bipy)(H₂O)₂]_n **1a** and rehydrated {[Cd(C₄O₄)(bipy)(H₂O)₂]}·3H₂O)_n **1b** during the reversible thermal re-/dehydration processes. It is also worthy to note that the dehydrated **1a** selectively adsorbs CO₂ over N₂. Moreover, the high water adsorption uptake of the dehydrated **1a** is attributed to the strong hydrogen-bonding affinity of water molecules with the uncoordinated O atoms of the squarate ligands in the host framework.

Acknowledgments: The authors wish to thank the Ministry of Science and Technology and Soochow University, Taiwan for financial support.

Author Contributions: Chih-Chieh Wang conceived and designed the experiments; Szu-Yu Ke, Kuan-Ting Chen, Tzu-Heng Wang, and Yi-Fang Hsieh performed the experiments, including synthesis, structural characterization, EA, IR, TG analysis, and gas-absorption measurements of compounds; Gene-Hsiang Lee contributed to the single-crystal X-ray data collection and structural analysis of compounds **1**; Yu-Chun Chuang contributed to the powder X-ray diffraction measurements of compound **1** by synchrotron radiation; and Chih-Chieh Wang and Yu-Chun Chuang wrote the paper.

Conflicts of Interest: The authors declare no conflict of interest.

References

1. Batten, S.R.; Champness, N.R.; Chen, X.M.; Garcia-Martinez, J.; Kitagawa, S.; Öhrström, L.; O’Keeffe, M.; Suh, M.P.; Reedijk, J. Terminology of metal-organic frameworks and coordination polymers. *Pure Appl. Chem.* **2013**, *85*, 1715–1724. [[CrossRef](#)]
2. Batten, S.R.; Champness, N.R.; Chen, X.M.; Garcia-Martinez, J.; Kitagawa, S.; Öhrström, L.; O’Keeffe, M.; Suh, M.P.; Reedijk, J. Coordination polymers, metal-organic frameworks and the need for terminology guidelines. *CrystEngComm* **2012**, *14*, 3001–3004. [[CrossRef](#)]
3. Li, B.; Chrzanowski, M.; Zhang, Y.; Ma, S. Applications of metal-organic frameworks featuring multi-functional sites. *Coord. Chem. Rev.* **2016**, *307*, 106–129. [[CrossRef](#)]
4. Zhang, X.; Wang, W.; Hu, Z.; Wang, G.; Uvdal, K. Coordination polymers for energy transfer: Preparations, properties, sensing applications, and perspectives. *Coord. Chem. Rev.* **2015**, *284*, 206–235. [[CrossRef](#)]
5. Bradshaw, D.; Claridge, J.B.; Cussen, E.J.; Prior, T.J.; Rosseinsky, M.J. Design, Chirality, and Flexibility in Nanoporous Molecule-Based Materials. *Acc. Chem. Res.* **2015**, *38*, 273–282. [[CrossRef](#)] [[PubMed](#)]
6. Silva, P.; Vilela, S.M.F.; Tome, J.P.C.; Paz, F.A.A. Multifunctional metal-organic frameworks: From academia to industrial applications. *Chem. Soc. Rev.* **2015**, *44*, 6774–6803. [[CrossRef](#)] [[PubMed](#)]

7. Li, S.; Huo, F. Metal-organic framework composites: From fundamentals to applications. *Nanoscale* **2015**, *7*, 7482–7501. [[CrossRef](#)] [[PubMed](#)]
8. Janiak, C.; Vieth, J.K. MOFs, MILs and more: Concepts, properties and applications for porous coordination networks (PCNs). *New J. Chem.* **2010**, *34*, 2366–2388. [[CrossRef](#)]
9. Serre, C.; Millange, F.; Thouvenot, C.; Nogues, M.; Marsolier, G.; Louër, D.; Forey, G. Very Large Breathing Effect in the First Nanoporous Chromium(III)-Based Slids: MIL-53 or CrIII(OH)·{O₂C–C₆H₄–CO₂}·{HO₂C–C₆H₄–CO₂H}_x·H₂O_y. *J. Am. Chem. Soc.* **2002**, *124*, 13519–13526. [[CrossRef](#)] [[PubMed](#)]
10. Kitaura, R.; Seki, K.; Akiyama, G.; Kitagawa, S. Porous coordination-polymer crystals with gated channels specific for supercritical gases. *Angew. Chem. Int. Ed.* **2003**, *42*, 428–431. [[CrossRef](#)] [[PubMed](#)]
11. Loiseau, T.; Serre, C.; Huguenard, C.; Fink, G.; Taulelle, F.; Henry, M.; Bataille, T.; Forey, G. A rationale for the large breathing of the porous aluminum terephthalate (MIL-53) upon hydration. *Chem. Eur. J.* **2004**, *10*, 1373–1382. [[CrossRef](#)] [[PubMed](#)]
12. Yamada, K.; Yagishita, S.; Tanaka, H.; Tohyama, K.; Adachi, K.; Kaizaki, S.; Kumagai, H.; Inoue, K.; Kitaura, R.; Chang, H.C.; et al. Metal-Complex Assemblies Constructed from the Flexible Hinge-Like Ligand H₂bhnq: Structural Versatility and Dynamic Behavior in the Solid State. *Chem. Eur. J.* **2004**, *10*, 2647–2660. [[CrossRef](#)] [[PubMed](#)]
13. Takamizawa, S.; Nakata, E.; Saito, T.; Kojima, K. Structural determination of physisorbed sites for CO₂ and Ar gases inside an organometallic framework. *CrystEngComm* **2003**, *5*, 411–413. [[CrossRef](#)]
14. Takamizawa, S.; Nakata, E.; Yokoyama, H.; Mochizuki, K.; Mori, W. Carbon dioxide inclusion phases of a transformable 1D coordination polymer host [Rh₂(O₂CPh)₄(pyz)]_n. *Angew. Chem. Int. Ed.* **2003**, *42*, 4331–4334. [[CrossRef](#)] [[PubMed](#)]
15. Takamizawa, S.; Nakata, E.; Saito, T. Gas inclusion crystal between 1-D coordination polymer and nitrous oxide: Occurrence of crystal phase transition induced by a slight amount of fluid guests inside host. *Inorg. Chem. Commun.* **2003**, *6*, 1415–1418. [[CrossRef](#)]
16. Takamizawa, S.; Nakata, E.; Saito, T. Single-crystal adsorbents: A new observation field for light aggregates. *Angew. Chem. Int. Ed.* **2004**, *43*, 1368–1371. [[CrossRef](#)] [[PubMed](#)]
17. Takamizawa, S.; Nakata, E.; Saito, T. Structural determination of copper(II) benzoate–pyrazine containing carbon dioxide molecules. *Inorg. Chem. Commun.* **2004**, *7*, 1–3. [[CrossRef](#)]
18. Takamizawa, S.; Nakata, E.; Saito, T. Saito, Inclusion Formation between 1D Coordination Polymer Host and CS₂ through Vapor Adsorption. *Chem. Lett.* **2004**, *33*, 538–539. [[CrossRef](#)]
19. Takamizawa, S.; Nakata, E. Direct observation of H₂ adsorbed state within a porous crystal by single crystal X-ray diffraction analysis. *CrystEngComm* **2005**, *7*, 476–479. [[CrossRef](#)]
20. Takamizawa, S.; Nakata, E.; Saito, T.; Akatsuka, T. Generation of a Plastic Crystal Including Methane Rotator within Metal-Organic Cavity by Forcible Gas Adsorption. *Inorg. Chem.* **2005**, *44*, 1362–1366. [[CrossRef](#)] [[PubMed](#)]
21. Takamizawa, S.; Nakata, E.; Akatsuka, T. Magnetic Behavior of a 1D Molecular-Oxygen System Included within a Transformable Single-Crystal Adsorbent. *Angew. Chem. Int. Ed.* **2006**, *45*, 2216–2221. [[CrossRef](#)] [[PubMed](#)]
22. Kawano, M.; Kobayashi, Y.; Ozeki, T.; Fujita, M. Direct Crystallographic Observation of a Coordinatively Unsaturated Transition-Metal Complex in situ Generated within a Self-Assembled Cage. *J. Am. Chem. Soc.* **2006**, *128*, 6558–6559. [[CrossRef](#)] [[PubMed](#)]
23. Yoshizawa, M.; Tamura, M.; Fujita, M. Diels-alder in aqueous molecular hosts: Unusual regioselectivity and efficient catalysis. *Science* **2006**, *312*, 251–254. [[CrossRef](#)] [[PubMed](#)]
24. Kachi-Terajima, C.; Akatsuka, T.; Kohbara, M.; Takamizawa, S. Structural and Magnetic Study of N₂, NO, NO₂, and SO₂ Adsorbed within a Flexible Single-Crystal Adsorbent of [Rh₂(bza)₄(pyz)]_n. *Chem. Asian J.* **2007**, *2*, 40–50. [[CrossRef](#)] [[PubMed](#)]
25. Takamizawa, S.; Kachi-Terajima, C.; Akatsuka, T.; Kohbara, M.; Jin, T. Alcohol-Vapor Inclusion in Single-Crystal Adsorbents [MII₂(bza)₄(pyz)]_n (M = Rh, Cu): Structural Study and Application to Separation Membranes. *Chem. Asian J.* **2007**, *2*, 837–848. [[CrossRef](#)] [[PubMed](#)]
26. Takamizawa, S.; Akatsuka, T.; Ueda, T. Gas-Conforming Transformability of an Ionic Single-Crystal Host Consisting of Discrete Charged Components. *Angew. Chem. Int. Ed.* **2008**, *47*, 1689–1692. [[CrossRef](#)] [[PubMed](#)]

27. Takamizawa, S.; Kohbara, M.; Akatsuka, T.; Miyake, R. Gas-adsorbing ability of tris-ethylenediamine metal complexes (M = Co(III), Cr(III), Rh(III), Ir(III)) as transformable ionic single crystal hosts. *New J. Chem.* **2008**, *32*, 1782–1787. [[CrossRef](#)]
28. Pan, Q.H.; Li, J.Y.; Chen, Q.; Han, Y.D.; Chang, Z.; Song, W.C.; Bu, X.H. [Co(en)₃]_{1/3}[In(ox)₂]₂·3.5H₂O: A zeolitic metal-organic framework templated by Co(en)₃Cl₃. *Microporous Mesoporous Mater.* **2010**, *132*, 453–457. [[CrossRef](#)]
29. Pan, Q.H.; Chen, Q.; Song, W.C.; Hu, T.L.; Bu, X.H. Template-directed synthesis of three new open-framework metal(II) oxalates using Co(III) complex as template. *CrystEngComm* **2010**, *12*, 4198–4204. [[CrossRef](#)]
30. Bertani, R.; Sgarbossa, P.; Venzo, A.; Lejl, F.; Amati, M.; Resnati, G.; Pilati, T.; Metrangolo, P.; Terraneo, G. Halogen bonding in metal-organic-supramolecular networks. *Coord. Chem. Rev.* **2010**, *254*, 677–695. [[CrossRef](#)]
31. Ingleson, M.J.; Bacsá, J.; Rosseninsky, M.J. Homochiral H-bonded proline based metal organic frameworks. *Chem. Commun.* **2007**, 3036–3038. [[CrossRef](#)] [[PubMed](#)]
32. Wang, C.C.; Yang, C.C.; Yeh, C.T.; Ceng, K.Y.; Chang, P.C.; Ho, M.L.; Lee, G.H.; Shih, W.J.; Sheu, H.S. Reversible Solid-State Structural Transformation of a 1D–2D Coordination Polymer by Thermal De/Rehydration Processes. *Inorg. Chem.* **2011**, *50*, 597–603. [[CrossRef](#)] [[PubMed](#)]
33. Desiraju, G.R. C–H···O and other weak hydrogen bonds. From crystal engineering to virtual screening. *Chem. Commun.* **2005**, 2995–3001. [[CrossRef](#)] [[PubMed](#)]
34. García-Báez, E.V.; Martínez-Martínez, F.J.; Höpfl, H.; Padilla-Martínez, I.I. π -Stacking Interactions and CH···X (X = O, Aryl) Hydrogen Bonding as Directing Features of the Supramolecular Self-Association in 3-Carboxy and 3-Amido Coumarin Derivatives. *Cryst. Growth Des.* **2003**, *3*, 35–45. [[CrossRef](#)]
35. Jabiak, C. A critical account on π – π stacking in metal complexes with aromatic nitrogen-containing ligands. *Dalton Trans.* **2000**, 3885–3896. [[CrossRef](#)]
36. Claessens, C.G.; Stoddart, J.F. π – π Interaction in self-assembly. *J. Phys. Org. Chem.* **1997**, *10*, 254–272. [[CrossRef](#)]
37. Guo, H.; Guo, X.; Batten, S.R.; Song, J.; Song, S.; Dang, S.; Zhang, G.; Tang, J.; Zhang, H. Hydrothermal Synthesis, Structures, and Luminescent Properties of Seven d¹⁰ Metal-Organic Frameworks Based on 9,9-Dipropylfluorene-2,7-Dicarboxylic Acid (H₂DFDA). *Cryst. Growth Des.* **2009**, *9*, 1394–1401. [[CrossRef](#)]
38. Reger, D.L.; Horger, J.J.; Smith, M.D.; Long, G.J.; Grandjean, F. Homochiral, Helical Supramolecular Metal-Organic Frameworks Organized by Strong π ··· π Stacking Interactions: Single-Crystal to Single-Crystal Transformations in Closely Packed Solids. *Inorg. Chem.* **2011**, *50*, 686–704. [[CrossRef](#)] [[PubMed](#)]
39. Wang, C.C.; Yang, C.C.; Chung, W.C.; Lee, G.H.; Ho, M.L.; Yu, Y.C.; Chung, M.W.; Sheu, H.S.; Shih, C.H.; Cheng, K.Y.; et al. A New Coordination Polymer Exhibiting Unique 2D Hydrogen-Bonded (H₂O)₁₆ Ring Formation and Water-Dependent Luminescence Properties. *Chem. Eur. J.* **2011**, *17*, 9232–9241. [[CrossRef](#)] [[PubMed](#)]
40. Kawamura, A.; Greenwood, A.R.; Filatov, A.S.; Gallagher, A.T.; Galli, G.; Anderson, J.S. Incorporation of Pyrazine and Bipyridine Linkers with High-Spin Fe(II) and Co(II) in a Metal-Organic Framework. *Inorg. Chem.* **2017**, *56*, 3349–3356. [[CrossRef](#)] [[PubMed](#)]
41. Kondo, A.; Satomi, T.; Azuma, K.; Takeda, R.; Maeda, K. New layered copper 1,3,5-benzenetriphosphonates pillared with N-donor ligands: Their synthesis, crystal structures, and adsorption properties. *Dalton Trans.* **2015**, *44*, 12717–12725. [[CrossRef](#)] [[PubMed](#)]
42. Botezat, O.; van Leusen, J.; Kravtsov, V.C.; Filippova, I.G.; Hauser, J.; Speldrich, M.; Hermann, R.P.; Kramer, K.W.; Liu, S.X.; Decurtins, S. Interpenetrated (8,3)-c and (10,3)-b Metal-Organic Frameworks Based on {Fe-3(III)} and {(Fe₂CoII)-Co-III} Pivalate Spin Clusters. *Cryst. Growth Des.* **2014**, *14*, 4721–4728. [[CrossRef](#)]
43. Wang, F.; Jing, X.M.; Zheng, B.; Li, G.H.; Zeng, G.; Huo, Q.S.; Liu, Y.L. Four Cd-Based Metal-Organic Frameworks with Structural Varieties Derived from the Replacement of Organic Linkers. *Cryst. Growth Des.* **2013**, *13*, 3522–3527. [[CrossRef](#)]
44. Thuery, P. Sulfonate Complexes of Actinide Ions: Structural Diversity in Uranyl Complexes with 2-Sulfobenzoate. *Inorg. Chem.* **2013**, *52*, 435–447. [[CrossRef](#)] [[PubMed](#)]
45. Gao, C.Y.; Liu, S.X.; Xie, L.H.; Sun, C.Y.; Cao, J.F.; Ren, Y.H.; Feng, D.; Su, Z.M. Rational design microporous pillared-layer frameworks: Syntheses, structures and gas sorption properties. *CrystEngComm* **2009**, *11*, 177–182. [[CrossRef](#)]

46. Mao, H.Y.; Zhang, C.H.; Li, G.; Zhang, H.Y.; Hou, H.W.; Li, L.K.; Wu, Q.G.; Zhu, Y.; Wang, E.B. New types of the flexible self-assembled Metal-Organic coordination polymers constructed by aliphatic dicarboxylates and rigid bidentate nitrogen ligands. *Dalton Trans.* **2004**, *22*, 3918–3925. [[CrossRef](#)] [[PubMed](#)]
47. Batten, S.R.; Murray, K.S. Structure and magnetism of coordination polymers containing dicyanamide and tricyanomethanide. *Coord. Chem. Rev.* **2003**, *246*, 103–130. [[CrossRef](#)]
48. Tong, M.L.; Ye, B.H.; Cai, J.W.; Chen, X.M.; Ng, S.W. Clathration of Two-Dimensional Coordination Polymers: Synthesis and Structures of $[M(4,4'\text{-bpy})_2(\text{H}_2\text{O})_2](\text{ClO}_4)_2 \cdot (2,4'\text{-bpy})_2 \cdot \text{H}_2\text{O}$ and $[\text{Cu}(4,4'\text{-bpy})_2(\text{H}_2\text{O})_2](\text{ClO}_4)_4 \cdot (4,4'\text{-H}_2\text{Bpy})$ ($M = \text{CdII}$, ZnII and $\text{bpy} = \text{Bipyridine}$). *Inorg. Chem.* **1998**, *37*, 2645–2650. [[CrossRef](#)] [[PubMed](#)]
49. Näther, C.; Greve, J.; Jeß, I. New Coordination Polymer Changing Its Color upon Reversible Deintercalation and Reintercalation of Water: Synthesis, Structure, and Properties of Poly[Diaqua- $(\mu_2$ -Squarato-O,O')- $(\mu_{2-4},4'$ -Bipyridine- N,N')- Manganese(II)] Trihydrate. *Chem. Mater.* **2002**, *14*, 4536–4542. [[CrossRef](#)]
50. Greve, J.; Jeß, I.; Näther, C.J. Synthesis, crystal structures and investigations on the dehydration reaction of the new coordination polymers poly[diaqua- $(\mu_2$ -squarato-O,O')- $(\mu_{2-4},4'$ -bipyridine- N,N')Me(II)] hydrate ($\text{Me} = \text{Co}$, Ni , Fe). *Solid State Chem.* **2003**, *175*, 328–340. [[CrossRef](#)]
51. Konar, S.; Corbella, M.; Zangrando, E.; Ribas, J.N.; Chaudhuri, R. The first unequivocally ferromagnetically coupled squarato complex: Origin of the ferromagnetism in an interlocked 3D Fe(II) system. *Chem. Commun.* **2003**, 1424–1425. [[CrossRef](#)]
52. Wang, C.C.; Yang, C.H.; Tseng, S.M.; Lee, G.H.; Sheu, H.S.; Phyu, K.W. A New Moisture-Sensitive Metal-Coordination Solids, $\{[\text{Cd}(\text{C}_4\text{O}_4)(\text{bipy})(\text{H}_2\text{O})_2] \cdot 3\text{H}_2\text{O}\}_\infty$ ($\text{bipy} = 4,4'\text{-bipyridine}$). *Inorg. Chim. Acta* **2004**, *357*, 3759–3764.
53. Ito, M.; West, R. New Aromatic Anions. IV. Vibrational Spectra and Force Constants for $\text{C}_4\text{O}_4^{2-}$ and $\text{C}_5\text{O}_5^{2-}$. *J. Am. Chem. Soc.* **1963**, *85*, 2580–2584. [[CrossRef](#)]
54. Blatov, V.A.; Shevchenko, A.P.; Serezhkin, V.N. TOPOS3.2: A new version of the program package for multipurpose crystal-chemical analysis. *J. Appl. Crystallogr.* **2000**, *33*, 1193. [[CrossRef](#)]
55. Blatov, V.A.; Carlucci, L.; Ciani, G.; Proserpio, D.M. Interpenetrating metal-organic and inorganic 3D networks: A computer-aided systematic investigation. Part I. Analysis of the Cambridge structural database. *CrystEngComm* **2004**, *6*, 377–395. [[CrossRef](#)]
56. Smart, V. *4.043 Software for CCD Detector System*; Siemens Analytical Instruments Division: Madison, WI, USA, 1995.
57. Saint, V. *4.035 Software for CCD Detector System*; Siemens Analytical Instruments Division: Madison, WI, USA, 1995.
58. Sheldrick, G.M. *Program for the Refinement of Crystal Structures*; University of Göttingen: Göttingen, Germany, 1993.
59. Sheldrick, G.M. *SHELXTL 5.03 (PC-Version), Program Library for Structure Solution and Molecular Graphics*; Siemens Analytical Instruments Division: Madison, WI, USA, 1995.



© 2017 by the authors. Licensee MDPI, Basel, Switzerland. This article is an open access article distributed under the terms and conditions of the Creative Commons Attribution (CC BY) license (<http://creativecommons.org/licenses/by/4.0/>).